ADVANCED MATERIALS
www.advmat.de

Controllable Formation of Luminescent Carbon Quantum Dots Mediated by the Fano Resonances Formed in Oligomers of Gold Nanoparticles

Yunbao Zheng, Haiying Liu, Jinxiang Li, Jin Xiang, Mingcheng Panmai, Qiaofeng Dai, Yi Xu, Shaolong Tie, and Sheng Lan**

Rapid and controllable formation of fluorescent carbon quantum dots (CQDs) is highly desirable in the fields of nanophotonics and biophotonics. Here, a novel strategy for creating CQDs, which emit white light efficiently under the excitation of either laser light or a mercury lamp, is proposed and demonstrated. The luminescent CQDs are generated by irradiating a poly(vinyl alcohol) (PVA) film doped with dense gold nanoparticles (AuNPs) with femtosecond laser pulses. The creation of CQDs from PVA is a two-step dehydration process mediated by AuNPs which act not only as heat sources but also as catalytic agents. The formation of C=C, C—C, and C—O bonds is confirmed by infrared Fourier transformation spectroscopy and X-ray photoelectron spectroscopy. It is revealed both numerically and experimentally that a spatially localized temperature distribution at the deep subwavelength scale can be achieved in oligomers of AuNPs by resonantly exciting the Fano resonances formed in the oligomers of AuNPs, enabling the generation of CQDs with small diameters. As one of the potential applications, it is demonstrated that optical display and optical data storage with ultralow energy can be realized by selectively introducing luminescent CQDs in the AuNP/PVA film.

Y. Zheng, Dr. H. Liu, J. Li, J. Xiang, M. Panmai, Dr. Q. Dai, Prof. S. Lan
Guangdong Provincial Key Laboratory of Nanophotonic Functional Materials and Devices
School of Information and Optoelectronic Science and Engineering
South China Normal University
Guangzhou 510006, P. R. China
E-mail: slan@scnu.edu.cn

Y. Zheng
School of Optoelectronic Engineering
Guangdong Polytechnic Normal University
Guangzhou 510665, P. R. China

Dr. Y. Xu
Department of Electronic Engineering
College of Information Science and Technology
Jinan University
Guangzhou 510632, P. R. China

Prof. S. Tie
School of Chemistry and Environment
South China Normal University
Guangzhou 510006, P. R. China
E-mail: tiesl@scnu.edu.cn

The ORCID identification number(s) for the author(s) of this article can be found under https://doi.org/10.1002/adma.201901371.

DOI: 10.1002/adma.201901371

Carbonic nanomaterials such as nanodiamonds, fullerenes, carbon nanotubes, graphene sheets, and carbon quantum dots (CQDs) have attracted extensive research efforts because of their unique properties and great potential for a wide variety of applications.[1–7] The accidental discovery of CQDs during the separation and purification of single-walled carbon nanotubes triggered subsequent studies to exploit the fluorescence properties of CQDs which comprise discrete nanoparticles with diameters below 10 nm and contain considerable amounts of carboxyl moieties at their surfaces.[8] Fluorescent CQDs are considered as the most promising candidates for replacing semiconductor quantum dots containing heavy metals in bioimaging because of their low toxicity, biocompatibility, low cost, and chemical inertness.[9–14] In addition, the large amounts of carboxyl moieties on the surfaces of CQDs impart excellent water solubility and suitable chemically reactive groups for surface passivation and functionalization. Moreover, the interesting photoinduced electron transfer properties of CQDs would offer exciting opportunities for light energy conversion, photovoltaic devices, and related applications.[1,15–17]

Basically, CQDs can be synthesized by either the top-down route or the bottom-up one.[18–21] So far, the production of CQDs via laser ablation of a carbon target has become a very important method and the synthesis of fluorescent CQDs by laser irradiation of a suspension of carbon materials in organic solvent has been demonstrated.[22–24] By properly selecting organic solvents, the surface states of CQDs could be modified to achieve tunable light emission and the origin of the luminescence was attributed to the surface states related to the ligands on the surfaces of CQDs. A review of the fabrication methods for CQDs, however, reveals some common limitations such as the long production time and the low controllability of the formed CQDs because only colloid CQDs are obtained. From the viewpoint of many practical applications, including but not limited to optical data storage, optical displays, and biosensing, the rapid and controllable formation of CQDs and especially CQD arrays is highly desirable.

In recent years, gold nanoparticles (AuNPs) and nanostructures have attracted great interest primarily due to their unique plasmonic properties. The catalytic researchers were long misled by this common sense until the exciting discovery that gold possesses unique catalytic activity in the oxidative elimination of carbon monoxide, carbon–carbon bond formation reactions, and so on.[25] Typically, a smaller nanoparticle tends to show a higher catalytic activity because of its larger surface-to-volume ratio.[26,27] The catalytic role of AuNPs in glucose oxidation was investigated and it was found that only exposed atoms are catalytically active.[28] It was shown that AuNPs supported on aluminum oxyhydroxide was active for aerobic oxidation of alcohol and sequential carbon–carbon bond formation with ketone.[29] More interestingly, the surface plasmon resonances (SPRs) of AuNPs can be used to drive catalysis reactions.[30–32]

Herein, we propose a novel strategy, in which the strongly localized temperature distribution created at the Fano resonances of the oligomers of AuNPs, plays a crucial role for the controllable formation of luminescent CQDs. The CQDs were accurately created in a poly(vinyl alcohol) (PVA) film doped with AuNPs by focused femtosecond laser light with appropriate pulse energy and irradiation time. They can emit strong white light with a broadband under the excitation of a continuous wave laser, a femtosecond laser, or even a mercury lamp. The formation of C—C and C=C bonds was confirmed by near-infrared Fourier transformation spectroscopy and X-ray photoelectron spectroscopy. As one of the possible applications, we demonstrated the use of such CQDs for high-density optical data storage. The arrays of CQDs can also serve as nanoscale light sources and chemical/biological sensors.

The principle of producing CQDs in a AuNP/PVA film by using femtosecond laser light is schematically shown in **Figure 1**a,b. Basically, the creation of CQDs from PVA is a chemical process mediated by AuNPs which act not only as heat sources but also as catalytic agents. In principle, it involves a two-step dehydration process. Upon the irradiation of femtosecond laser pulses, the electrons in AuNPs are excited to the high-energy states and the thermalization of hot electrons causes the temperature rise of AuNPs and the surrounding environment. Once the environment temperature becomes higher than 160 °C, the intramolecular dehydration of PVA molecules occurs, leading to the formation of CQDs in the vicinity of AuNPs. The chemical reaction equations responsible for the formation of CQDs can be described as follows

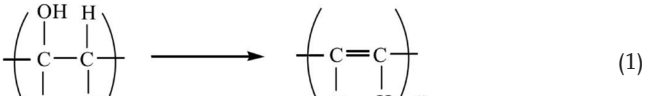
(1)

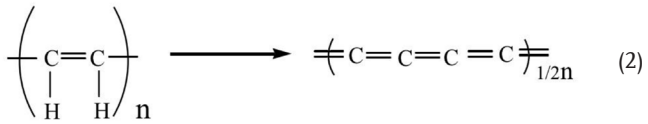
(2)

In the first step, the dehydration occurs at a sufficiently high temperature. After that, the second dehydration process happens in the presence of oxygen. The similar mechanism is applied to other polymers but the efficiencies for producing CQDs may be different. However, it is found that the catalytic role of AuNPs in the formation of CQDs is unique (Figures S1 and S2, Supporting Information).

As discussed above, carbon (C) clusters can be achieved through the dehydration of PVA. However, the size control is crucial in order to obtain CQDs with small diameters, which emit photons effectively in the visible light spectrum. Basically, the size of the C clusters is determined by the temperature distribution around AuNPs. Highly localized temperature distribution is required in order to obtain CQDs with small diameters. In a AuNP/PVA film formed by doping AuNPs with a large volume density in a PVA matrix, a large number of oligomers are expected to be created in which the constituent AuNPs are strongly coupled, forming plasmonic hot spots. Physically, the temperature distribution in an oligomer is affected by the plasmonic coupling between the constituent AuNPs. However, it can be much different from the electric field distribution in the oligomer. Therefore, it is necessary to clarify how the plasmonic coupling will influence the temperature distribution in an oligomer.

It has been known that a Fano resonance can be created in the extinction spectrum of an oligomer composed of seven identical gold nanospheres (AuNSs) (i.e., a heptamer).[33,34] The Fano resonance originates from the coherent interaction (interference) of the plasmonic modes excited in the oligomer. These modes arise mainly from the plasmonic coupling of the constituent AuNPs and usually appear at longer wavelengths of the SPR of AuNPs. Therefore, the Fano resonances of oligomers of AuNPs are generally observed at the longer wavelengths of the SPR of AuNPs.[34–36] The Fano resonance formed in the heptamer of AuNSs becomes significant with decreasing gap width among the AuNSs, implying that the plasmonic coupling plays a crucial role in the formation and tunability of the Fano resonance. From the electric field distribution calculated at the dip of the Fano resonance supported by the heptamer, one can see plasmonic hot spots with significantly enhanced electric field created at the gap regions between the AuNSs (Figure S3, Supporting Information). When we calculated the temperature distribution at the Fano dip, it was found that the temperature distribution in the heptamer is much different from the electric field distribution (Figure S3, Supporting Information). It is noticed that the temperature at the central AuNS is much higher than those in the surrounding AuNSs, leading to a highly localized temperature distribution. If we reduce the radius of the central AuNS from 7 to 3 nm, the Fano dip in the extinction spectrum becomes less pronounced because of the reduced plasmonic coupling between the central AuNS and the surrounding AuNSs. As a result, the temperature distribution at the Fano dip becomes delocalized (Figure S3, Supporting Information). Previously, the localization of excess temperature in plasmonic nanostructures has been systematically investigated and strongly localized temperature distribution has been achieved in AuNPs placed in the gap region of a nanoantenna by exploiting the effect of Fano resonance.[37]

In our case, AuNPs with a large size distribution were intentionally used to fabricate the AuNP/PVA film. From the transmission electron microscopy (TEM) images of the AuNPs shown in Figure 1c, it can be seen that the diameters of the AuNPs range from 2 to 20 nm. As a typical example,

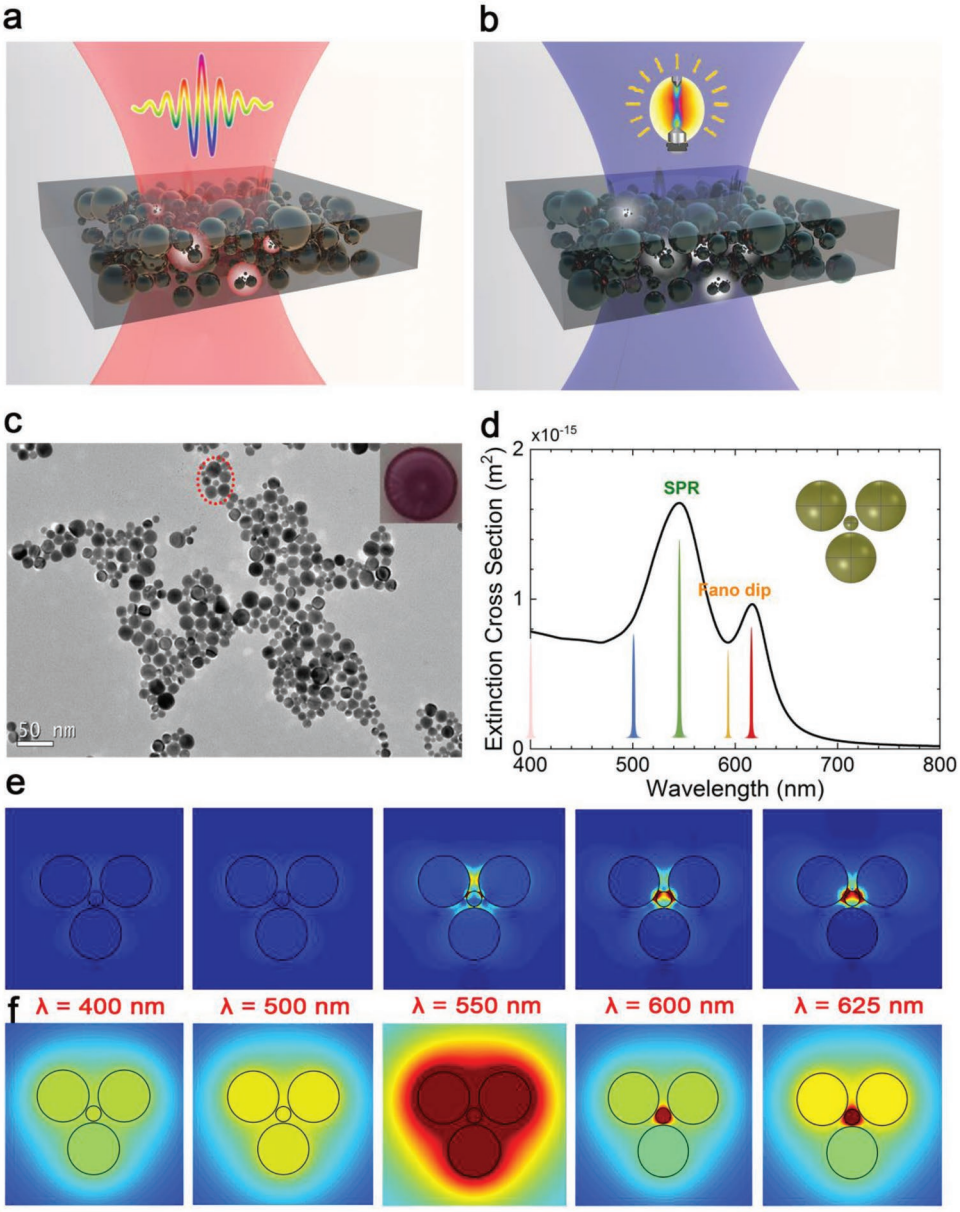

Figure 1. a) Schematic showing the controllable generation of CQDs in a AuNP/PVA composite irradiated by focused femtosecond laser light. b) Schematic showing the white light emitted from CQDs under the excitation of a mercury lamp. c) TEM images of the AuNPs used for the fabrication of AuNP/PVA composites. The inset shows the photo of the fabricated AuNP/PVA film. d) Extinction spectrum calculated for a tetramer composed of a AuNS with $d = 5$ nm surrounded by three AuNSs with $d = 17$ nm. The schematic of the tetramer is shown in the inset. The nearest gap width between the central AuNS and the surrounding ones was chosen to be $g = 1.0$ nm. The pulse symbols indicate the excitation wavelengths of the femtosecond laser light. The electric field and temperature distributions calculated for the tetramer which are excited at different wavelengths of 400, 500, 550, 600, and 625 nm are presented in (e) and (f), respectively. The incident plane wave is horizontally polarized.

we investigated numerically the effect of Fano resonance on the temperature distribution in a tetramer composed of four AuNSs, as shown in the inset of Figure 1d. The central AuNS has a smaller diameter of $d = 5$ nm as compared with the surrounding AuNSs ($d = 17$ nm). As expected, a pronounced Fano dip is observed at ≈600 nm in the extinction spectrum of the tetramer, as shown in Figure 1d. In Figure 1e,f, we present the electric field and temperature distributions calculated for the tetramer at different wavelengths of 400, 500, 550, 600, and 625 nm. For excitation wavelengths of 550, 600, and 625 nm, one can see significantly enhanced electric field achieved at the gaps between the central AuNS and the surrounding AuNSs. It is remarkable that the temperature distributions at 400, 500, and 550 nm appear to be uniform over the four AuNSs. In sharp contrast, the temperature in the central AuNS is much higher than those in the surrounding AuNSs when the Fano dip is resonantly excited at 600 nm, implying the achievement of highly localized temperature distribution in subwavelength spatial scale. At 625 nm where the Fano peak appears, a slight increase of the temperature in the upper two AuNSs is

observed. However, the temperature localization in the central AuNS remains nearly unchanged.

We have systematically investigated oligomers with different configurations and found that the Fano dip can be tuned in the wavelength range of 600–650 nm by varying the configuration parameters of the oligomer (Figure S4, Supporting Information). In addition, the wavelength for achieving the spatial temperature localization in the central AuNS of an oligomer extends widely from ≈600 to ≈680 nm. Since highly localized temperature distribution can be achieved no matter the wavelength of the incident light is chosen at the dip or the peak of the Fano resonance (see Figure 1f), the uniformities of both AuNPs and their oligomers have negligible influence on the formation of CQDs. In order to see the effect of Fano resonance on the formation of CQDs, we intentionally chose several irradiation wavelengths for the femtosecond laser light and compared their efficiencies in the fabrication of luminescent CQDs. These typical wavelengths are located in the short-wavelength side of the SPR of AuNPs (400, 450, and 500 nm), exactly at the SPR (550 nm), and in the long-wavelength side of the SPR (600 and 650 nm).

Since the temperature localizations achieved in different oligomers are different, the sizes of CQDs created in different oligomers are generally different, leading to the emissions with different wavelengths (or colors). As schematically shown in Figure 1b, one can expect white light emission from the assembly of randomly distributed CQDs. Since the refractive index change before and after the formation of CQDs is quite small, it is expected that most hot spots are still active after the formation of CQDs. As a result, the emission of CQDs will also be beneficial from the significantly enhanced electric field achieved at the Fano resonance.

Basically, the size and density of the formed CQDs depend strongly on the energy (or fluence) and irradiation time of the femtosecond laser pulses. Thus, these two parameters were used to optically control the formation of CQDs in our experiments. The fabricated CQDs with suitable size and density can emit strong luminescence under the excitation of a femtosecond laser with a lower pulse energy, a continuous wave laser with a short wavelength or even a mercury lamp.

We first examined the evolution of the luminescence spectrum of the AuNP/PVA film with increasing pulse energy when it was irradiated by using femtosecond laser pulses with different excitation wavelengths (λ_{ex}) of 400, 530, and 650 nm. A broad emission band covering the entire visible light spectrum was observed when the film was excited by using 400 nm femtosecond laser light with a small pulse energy of E_{ira} = 3.3 pJ (≈0.2 mJ cm^{-2}) and a fixed irradiation time of t = 1.0 s, as shown in **Figure 2**a. Initially, the luminescence intensity was found to increase with increasing pulse energy. For pulse energies larger than 29.6 pJ, however, a reduction of the luminescence intensity was observed. In addition, the luminescence peak was redshifted to ≈620 nm for E_{ira} > 16.5 pJ. When we fixed E_{ira} = 33 pJ and increased the irradiation time, a similar behavior was observed, as shown in Figure 2b. For t < 4.0 s, an increase of the luminescence intensity was seen. After that, the luminescence intensity began to decrease with increasing irradiation time. Similarly, the luminescence peak finally appeared at ≈620 nm. From the above experimental results, we speculated that CQDs were created upon the irradiation of the femtosecond laser light due to the heating of AuNPs with unique catalytic activity. The size of the formed CQDs depends strongly on the pulse energy and irradiation time of the femtosecond laser light. The higher the pulse energy or the longer the irradiation time, the larger the size and volume density of the formed CQDs are. For small pulse energies or short irradiation times, one can get small CQDs, which are highly luminescent. However, the density of the small CQDs is also low, leading to weak luminescence intensity. When a large pulse energy or a long irradiation time is employed, the volume density of the CQDs increases but their size also becomes larger, leading to a low quantum yield. As a result, the luminescence intensity may become weaker. For this reason, there exists an optimum pulse energy for a AuNPs/PVA film at which CQDs with the strongest luminescence intensity are obtained if the irradiation time is fixed (Figure S5, Supporting Information). Similarly, an optimum irradiation time is expected for a fixed pulse energy. Since CQDs are generated by the heat released from AuNPs and the absorption of AuNPs increases when the excitation wavelength approaches the SPR of AuNPs (≈530 nm), the pulse energy and irradiation time at which the luminescence intensity reaches its maximum value were decreased to E_{ira} = 23 pJ and t = 2.0 s when the excitation wavelength was changed from λ_{ex} = 400 nm to λ_{ex} = 530 nm, as shown in Figure 2c,d. When the excitation wavelength was further moved to λ_{ex} = 650 nm, the pulse energy and irradiation time at which the luminescence intensity begins to decrease were further reduced to be 16.5 pJ and 0.4 s (see Figure 2e,f), in good agreement with the strongly localized temperature distribution expected at the Fano resonance.

As mentioned above, the luminescence intensity of the CQDs is determined not only by the size of CQDs but also by their volume density, which depend strongly on the pulse energy and irradiation time. If the irradiation time is fixed, then one can find an optimum pulse energy at which the strongest luminescence from CQDs can be achieved. We have examined the luminescence spectra of the AuNP/PVA film, which was excited by using a sufficiently low pulse energy of E_{ira} = 0.33 pJ, before and after the irradiation of the 400 nm femtosecond laser light with different pulse energies and a fixed irradiation time of t = 1 s (Figure S5, Supporting Information). For a small pulse energy of E_{ira} = 0.66 pJ, the luminescence intensity was increased by a factor of ≈3.0 after the irradiation of the femtosecond laser light. When the pulse energy was raised to E_{ira} = 13.2 pJ, the enhancement factor for the luminescence intensity was increased dramatically to ≈48. A further increase of the pulse energy to E_{ira} = 39.5 pJ, however, led to a reduction of the enhancement factor to ≈4.0. In this case, it is thought that the size of most CQDs became much larger than 10 nm, quenching the luminescence in the visible light spectrum.

In **Figure 3**, we compared the changes in the luminescence spectra of the AuNP/PVA film before and after the irradiation of the femtosecond laser light with different wavelengths. The pulse energy and irradiation time used to create CQDs had been optimized so that a maximum enhancement factor was obtained in each case. A much smaller pulse energy of E_{det} = 0.33 pJ was employed to excite the luminescence of CQDs. For λ_{ex} = 400 nm, an enhancement factor as large as ≈48 was

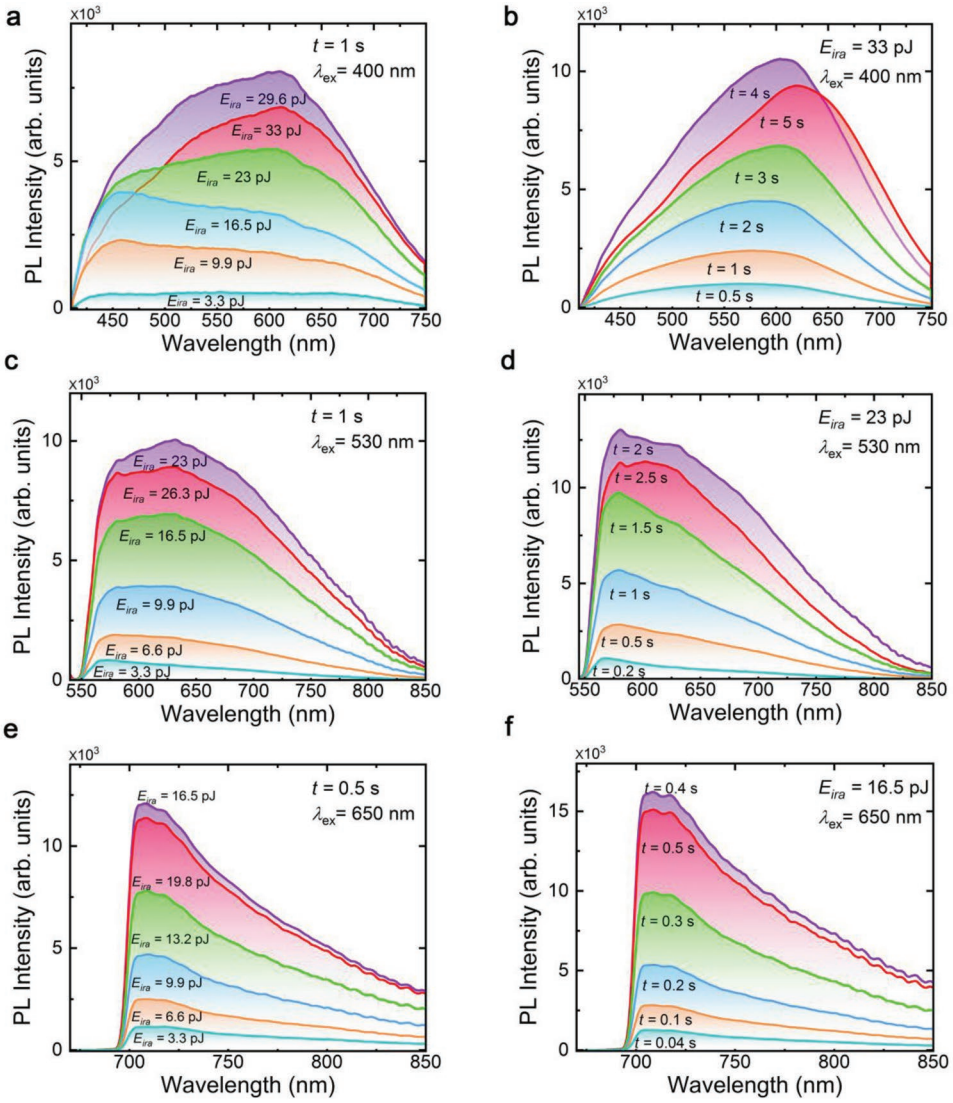

Figure 2. Evolution of the luminescence spectrum of the AuNP/PVA film with increasing pulse energy measured at different excitation wavelengths of 400 nm (a), 530 nm (c), and 650 nm (e). The evolution of the luminescence spectrum of the AuNP/PVA film, which was excited at a fixed pulse energy, with increasing irradiation time is shown in (b), (d), and (f) for excitation wavelengths of 400, 530, and 650 nm.

observed at ≈620 nm, as shown in Figure 3a. In comparison, a slight increase of the enhancement factor to ≈52 was achieved at ≈630 nm if the wavelength of the femtosecond laser light was set at λ_{ex} = 530 nm. The enhancement factor can be further increased to ≈56 when the film was irradiated by using femtosecond laser light at λ_{ex} = 650 nm. In Figure 3d, we show the luminescence spectra of a pure PVA film before and after the irradiation of the femtosecond laser light. It can be seen that no obvious change was found after the irradiation of the femtosecond laser light, verifying undoubtedly that the significant increase in the luminescence observed in the AuNP/PVA film was caused by the formation of luminescent CQDs. Since CQDs are created in the gap regions of AuNPs where many hot spots are expected to be present through plasmonic coupling (see Figure 1e), we need to consider the enhancement of the luminescence of CQDs by such hot spots. In order to evaluate the effect of localized electric field on the radiative recombination rate of CQDs (the so-called plasmonic Purcell effect), we measured the luminescence decay of CQDs by using 400 nm femtosecond laser pulses, as shown in the inset of Figure 3c. The two lifetimes extracted from the biexponential decay of the luminescence were found to be $\tau_1 \approx 0.5$ ns and $\tau_2 \approx 2.0$ ns. The shorter lifetime, which is only one-fourth of that reported for bare CQDs (≈2.0 ns),[38,39] is caused by the plasmonic Purcell effect. The longer one is the luminescence lifetime of CQDs which are not located at hot spots because the electric field distribution does not match the temperature distribution, as shown in Figure 1e,f. Therefore, we concluded that the luminescence of CQDs (radiative recombination rate) was enhanced by a factor of ≈4.0 owing to the existence of hot spots created by the plasmonic coupling of AuNPs.

Since PVA is an insulator which is not transparent to electron beam, the direct characterization of CQDs created in the PVA film by using TEM observation remains as a big

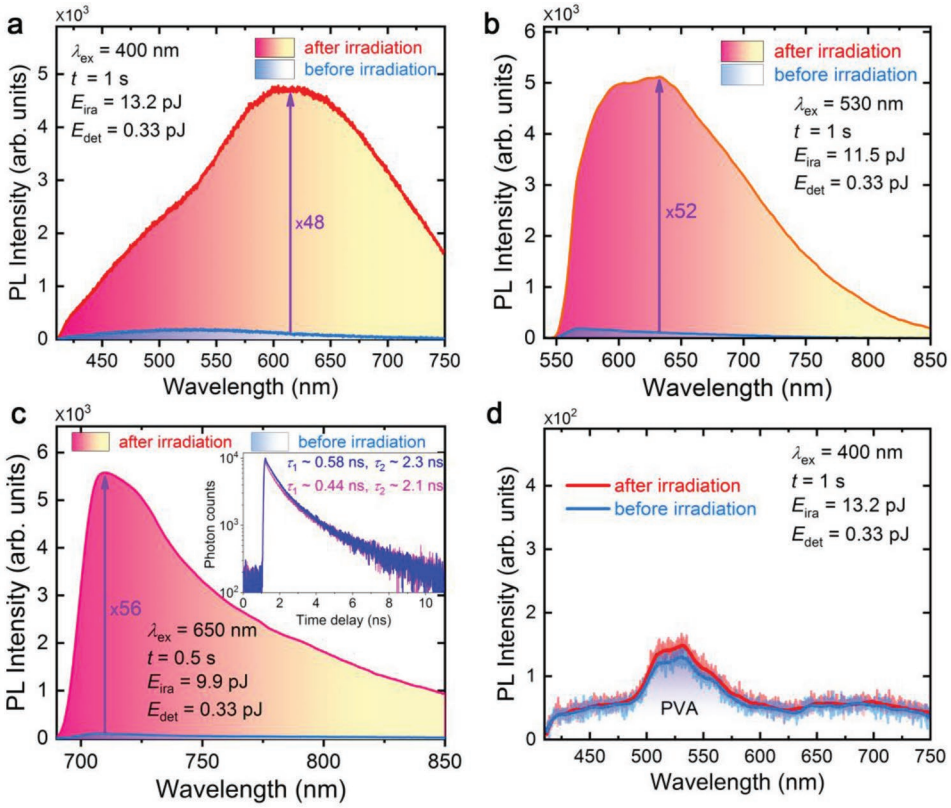

Figure 3. Comparison of the luminescence spectra of the Au/PVA film before and after the irradiation of femtosecond laser pulses with a pulse energy of 13.2 pJ (a), 11.5 pJ (b), and 9.9 pJ (c), respectively. A comparison of the luminescence spectra of the pure PVA film before and after the irradiation of femtosecond laser pulses with a pulse energy of 13. 2 pJ is shown in (d). In all cases, a much smaller pulse energy of 0.33 pJ was used to obtain the luminescence spectra. The luminescence decays measured for CQDs located at two different positions of the film (blue and pink curves) are shown in the inset of (c).

challenge. In order to further confirm the formation of CQDs, we compared the Fourier transformation spectra taken from the regions without and with the irradiation of femtosecond laser light, as shown in **Figure 4**a. In the transmission spectra, one can see transmission valleys located at 1154, 1496, 1628, and 2990 cm^{-1}, which are attributed to the characteristic absorptions of C−O, C−C, C=C, and C−H bonds, respectively. It is remarkable that the absorptions of all these bonds are enhanced after the irradiation of femtosecond laser light, especially for C−C and C=C bonds. It implies the formation of CQDs composed mainly of C−C and C=C bonds in the irradiated region.[40]

A further verification of the formation of CQDs was manifested in the X-ray photoelectron spectroscopy (XPS) carried out on the regions without and with the irradiation of femtosecond laser light, as shown in Figure 4b,c. In both cases, the XPS spectra can be decomposed into the contributions of C=C, C−O, and C=O bonds which are located at 284.6, 286.4, and 288.0 eV, respectively. As compared with the region without the irradiation of femtosecond laser light, the peak intensities of C=C, C−O, and C=O bonds in the region irradiated by femtosecond laser light were found to be increased by factors of 2.6, 1.4, and 1.6, respectively. This phenomenon indicates the formation of CQDs which possess more C=C and C−O bonds than PVA.[41,42]

For femtosecond laser light with wavelengths shorter than 530 nm, the temperature distributions in the oligomer of AuNPs are quite similar. However, the temperature rises in AuNPs are expected to increase when the wavelength of the femtosecond laser light approach the SPRs of AuNPs (see Figure 1e), so does the volume density of CQDs generated by using the same pulse energy. In **Figure 5**, we compare the images (a petunia) recorded by using femtosecond laser light with different wavelengths of 400, 450, and 500 nm and the same pulse energy of ≈13.2 pJ and extracted by using the bright-field mode of the microscope (Figure 5a–c), the 361 nm line of the mercury lamp (Figure 5d–f), and the 488 nm line (continuous wave) of a laser scanning confocal microscope (Figure 5g–i), respectively (see the Experimental Section for experimental details). For λ_{ex} = 400 nm, the recorded pattern was invisible under the bright-field mode of the microscope (see Figure 5c), implying the volume density of CQDs was quite small. The recorded pattern became visible for λ_{ex} = 450 nm and a much darker one was obtained at λ_{ex} = 500 nm. Under the excitation of the mercury lamp, the pattern recorded at λ_{ex} = 400 nm was still invisible. In contrast, the white light emitted from CQDs can be distinguished at λ_{ex} = 450 nm and the recorded information can be acquired at λ_{ex} = 500 nm. Similarly, one can clearly observe the patterns recorded at λ_{ex} = 450 and 500 nm under a laser scanning confocal microscope (see Figure 5g,h).

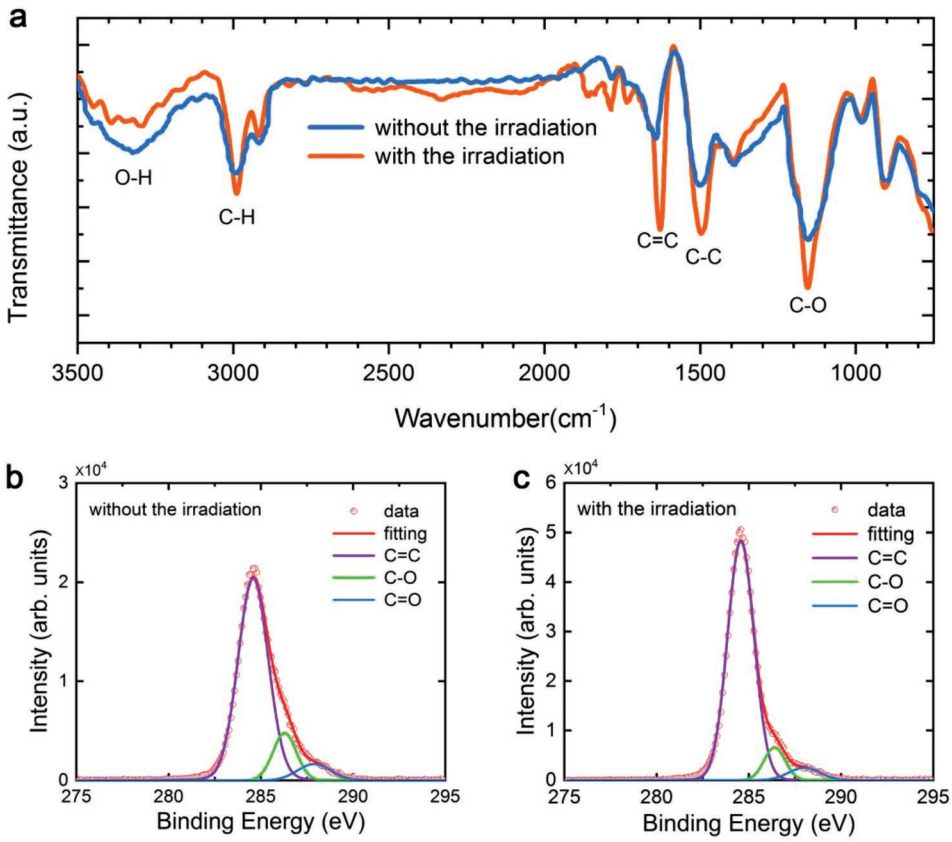

Figure 4. a) Near-infrared Fourier transformation spectra measured for the AuNP/PVA film without and with the irradiation of femtosecond laser light with a pulse energy of 13.2 pJ. The corresponding X-ray photoelectron spectroscopy measured for the AuNP/PVA film is shown in (b) and (c), respectively.

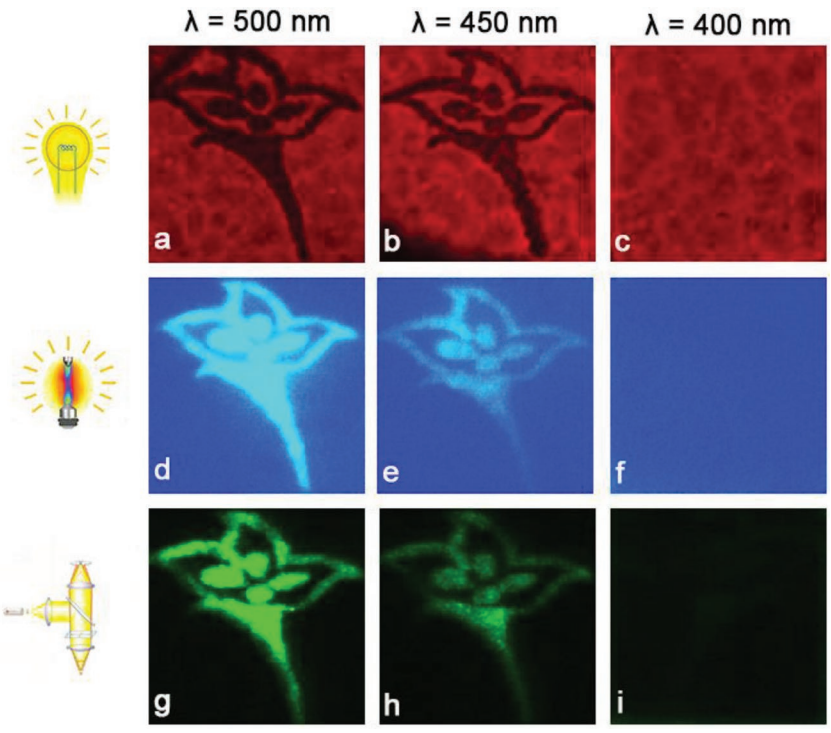

In **Figure 6**, we present a comparison of the images recorded at longer irradiation wavelengths of 530, 600, and 650 nm and acquired by using different methods. More experimental results by using femtosecond laser light with different wavelengths are presented in Supporting Information (see Figures S6–S14 in the Supporting Information). The image used for recording and readout is the LOGO of our school (School of Information and Optoelectric Science and Engineering of South China Normal University). From the image recorded at λ_{ex} = 530 nm and extracted by using the bright-field mode of the microscope, one can see the generation of dark CQDs. However, the generated CQDs did not produce a complete image. Accordingly, the images extracted by using the mercury lamp, the cw

Figure 5. Comparison of the images recorded at different wavelengths of 500, 450, and 400 nm and extracted by using the bright-field mode of the microscope (a–c), the 361 nm line of the mercury lamp (d–f), and the 488 nm line of a laser scanning confocal microscope (g–i).

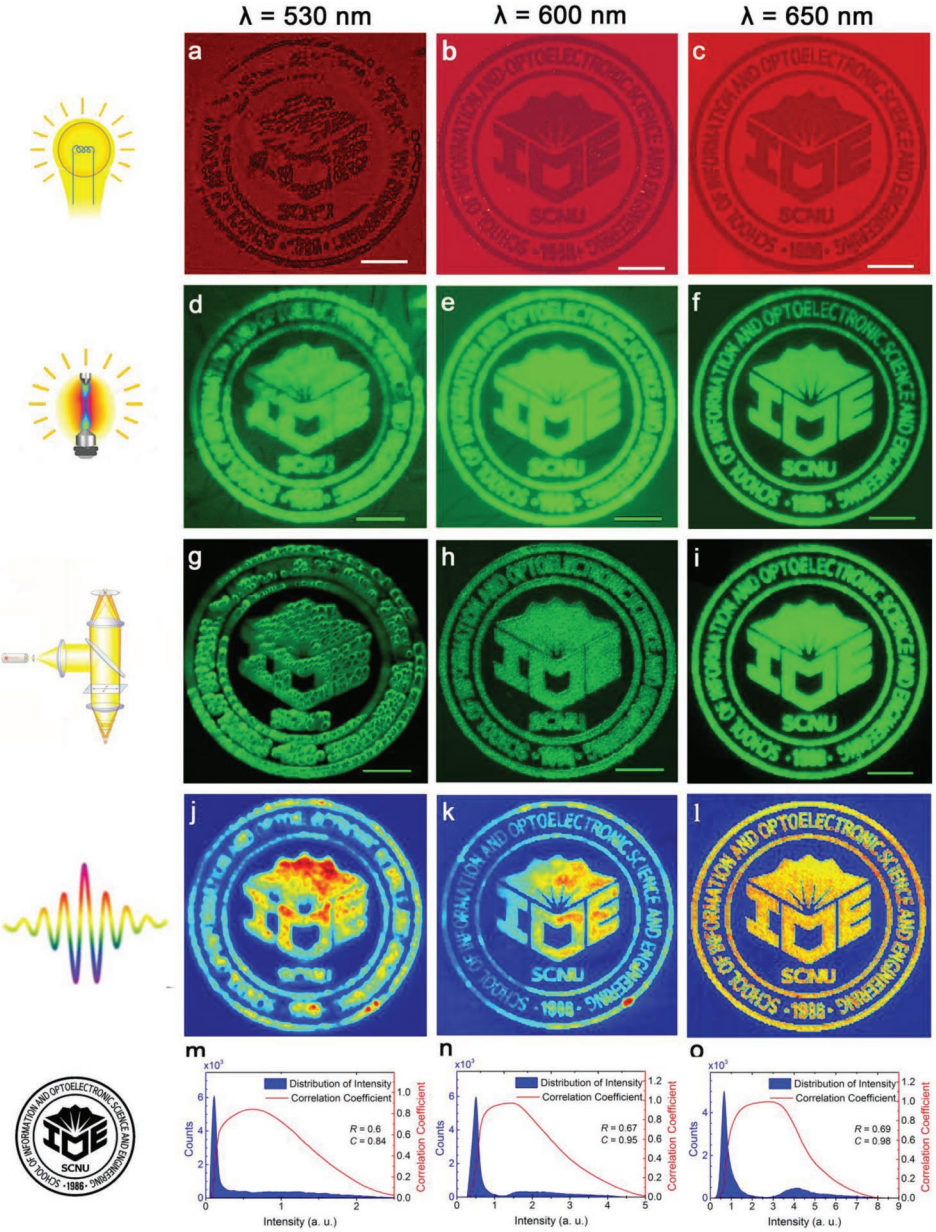

Figure 6. a–l) Comparison of the images recorded at different wavelengths of 530, 600, and 650 nm and extracted by using the bright-field mode of the microscope (a–c), the 465 nm line of the mercury lamp (d–f), the 488 nm line of a laser scanning confocal microscope (g–i), and the same femtosecond laser light with a lower pulse energy (j–l). The correlation coefficients (*C*) and contrasts (*R*) extracted for the images shown in (j–l) are presented in (m–o), respectively. The length of the scale bar in (a–l) is 50 µm.

laser light, and the femtosecond laser light appeared to be vague. A large number of dark spots, which correspond to the bright spots in the bright-field microscopy image, can be found in these light-emitting images. In comparison, the CQDs created at $\lambda_{ex} = 600$ and 650 nm gave rise to complete images quite similar to the original one. The physical origin for this behavior can be understood if we consider the temperature distributions created in the oligomers of AuNPs at different wavelengths discussed above. At $\lambda_{ex} = 530$ nm where the SPR of the AuNPs located, the largest temperature rise is expected because of the largest extinction cross section at this wavelength. However, spatially-localized temperature distribution is not obtained at this wavelength. As a result, CQDs with larger diameters, which do not emit light in the visible spectrum, would be generated at the centers of oligomers. Meanwhile, CQDs emitting visible light were produced at the edges of the oligomers. Thus, one can find many dark spots with bright edges in the images recorded at $\lambda_{ex} = 530$ nm when they were read out by using laser scanning confocal microscope. In sharp contrast, spatially-localized temperature distribution at deep subwavelength scale can be achieved for excitation wavelengths ranging from 600 to 650 nm owing to the Fano resonances formed in the oligomers of AuNPs. Consequently, CQDs with small diameters, which emit white light efficiently, can be created. Here, we

demonstrated that high-quality optical data storage can be realized by exploiting the strongly localized temperature distribution achieved at the Fano resonances, as shown in Figure 6f,i,l. From Figure 6o, it can be seen that the image extracted by using femtosecond laser light possesses a correlation coefficient as high as $C = 0.98$ and a contrast as large as $R = 0.69$, implying an extremely low error rate and ultrahigh quality in data storage (see Figure S15 in the Supporting Information)

In summary, we have proposed and demonstrated a new method to create CQDs which emit white light efficiently under the excitation of either laser light or mercury lamp. The luminescent CQDs were generated by irradiating the AuNP/PVA film with femtosecond laser pulses of appropriate pulse energy and irradiation time. The formation of C=C, C—C, and C—O bonds was confirmed by infrared Fourier transformation spectroscopy and X-ray photoneletron spectroscopy. It was revealed both numerically and experimentally that the Fano resonances formed in the oligomers of AuNPs play crucial roles in the generation of luminescent CQDs. The spatially-localized temperature distribution at deep subwavelength scale achieved in the oligomers of AuNPs at the Fano resonances enables the generation of CQDs with small diameters. The advantages of the proposed method over traditional ones include: 1) CQDs can be fabricated in a polymer matrix rather than in a solvent, 2) luminescent CQDs can be directly obtained without any surface passivation or decoration, 3) CQDs can be fabricated controllably in a polymer matrix, making it possible for creating CQD arrays for display and sensing applications, 4) the fabrication time is extremely short and CQDs can be immediately obtained upon the irradiation of femtosecond laser light, 5) the size and density of CQDs can be readily controlled by adjusting the power of the irradiated femtosecond laser light. The controllable generation of luminescent CQDs mediated by Fano resonances demonstrated in this work may find potential applications in the fields of nanophotonics and biophotonics. As one of potential applications, we showed that optical display and optical data storage with ultralow energy can be realized by selectively introducing luminescent CQDs in the AuNP/PVA film.

Experimental Section

Sample Preparation: AuNPs with diameters ranging from 2 to 20 nm were synthesized by using the modified seedless method.[43] PVA films doped by AuNPs with a large volume density of 10^9 cm^{-3} were prepared by mixing AuNPs with 5% PVA and spin coating the solution on a glass slide (see Figure S16 in the Supporting Information). Oligomers of AuNPs were formed during the evaporation of the solvent, which was water in this case, through the so called convective self-assembly.[44–46] The transmission spectra of the regions on the AuNP/PVA film with and without irradiation of femtosecond laser pulses were characterized by using an inverted microscope (Axio Observer A1, Zeiss) (see Figure S17 in the Supporting Information).

Experimental Setup: The femtosecond laser light with a repetition rate of 76 MHz and a duration of 130 fs was employed to irradiate the AuNP/PVA film and to excite the luminescence of CQDs. It was obtained by doubling the frequency of the 800 nm output of a femtosecond oscillator (Mira 900S, Coherent) with a BBO crystal or by directly employing an optical parametric oscillator (Mira OPO-X, Coherent). The femtosecond laser light was focused on the AuNP/PVA films by using the 60× objective lens (NA = 0.85) of an inverted microscope (Axio Observer A1, Zeiss). The generated optical signals were collected by using the same objective lens and directed to a spectrometer (SR-500i-B1, Andor) for analysis or to a coupled-charge device (DU970N, Andor) for recording. An electronic shutter was used to control the irradiation time. When measuring the luminescence lifetime of CQDs, they were excited by 400 nm femtosecond laser pulses and the luminescence decay at ≈600 nm was examined (PicoHarp 300, PicoQuant). For the fabrication of the arrays of CQDs and optical data storage, the AuNP/PVA film was placed on a 3D positioning system (P-563.3CD, Physik Instrument) with an accuracy of 1 nm in all three dimensions. The patterns recorded were extracted by using the same femtosecond laser light with a lower pulse energy or by using a laser scanning confocal microscope (A1, Nikon).

Numerical Modeling: The extinction spectra of the oligomers of AuNSs with different configurations and the electric field and temperature distributions in the oligomers were calculated numerically based on the finite element method (FEM) by using a commercially developed software (COMSOL Multiphysics v5.4). The numerical simulations were performed in a sphere whose diameter was set to be the wavelength of the incident light. The oligomers were placed at the center of a sphere which was enclosed by a perfectly matched layer capable of absorbing all the outgoing radiation. Tetrahedral meshes were used in the air region. The relative tolerance of the solver was slightly lowered to better capture the heat load. The temperature inside each AuNS was assumed to be uniform owing to the small size and good conductivity of gold.

Supporting Information

Supporting Information is available from the Wiley Online Library or from the author.

Acknowledgements

Y.Z. and H.L. contributed equally to this work. S.L. thanks the financial support from the National Key Research and Development Program of China (No. 2016YFA0201002). S.L., H.L., and S.T. acknowledge the financial support from the National Nature and Science Foundation of China (Grant Nos. 11674110 and 11874020), the Natural Science Foundation of Guangdong Province, China (Grant Nos. 2016A030308010 and 2018A030313854), and the Science and Technology Planning Project of Guangdong Province, China (Grant No. 2015B090927006).

Conflict of Interest

The authors declare no conflict of interest.

Keywords

carbon quantum dots, Fano resonances, femtosecond laser pulses, gold nanoparticles, optical data storage, poly(vinyl alcohol)

Received: March 1, 2019
Revised: May 13, 2019
Published online:

[1] S. N. Baker, G. A. Baker, *Angew. Chem., Int. Ed.* **2010**, *49*, 6726.
[2] H. Li, Z. Kang, Y. Liu, S.-T. Lee, *J. Mater. Chem.* **2012**, *22*, 24230.
[3] T. Gokus, R. R. Nair, A. Bonetti, M. Böhmler, A. Lombardo, K. S. Novoselov, A. K. Geim, A. C. Ferrari, A. Hartschuh, *ACS Nano* **2009**, *3*, 3963.
[4] G. Eda, Y.-Y. Lin, C. Mattevi, H. Yamaguchi, H.-A. Chen, I. S. Chen, C.-W. Chen, M. Chhowalla, *Adv. Mater.* **2010**, *22*, 505.

[5] J. Shen, Y. Zhu, X. Yang, C. Li, *Chem. Commun.* **2012**, *48*, 3686.
[6] G. Li, R. Jin, *Nanotechnol. Rev.* **2013**, *2*, 529.
[7] H. C. Wong, A. M. Higgins, A. R. Wildes, J. F. Douglas, J. T. Cabral, *Adv. Mater.* **2012**, *25*, 985.
[8] X. Xu, R. Ray, Y. Gu, H. J. Ploehn, L. Gearheart, K. Raker, W. A. Scrivens, *J. Am. Chem. Soc.* **2004**, *126*, 12736.
[9] L. Cao, X. Wang, M. J. Meziani, F. Lu, H. Wang, P. G. Luo, Y. Lin, B. A. Harruff, L. M. Veca, D. Murray, S.-Y. Xie, Y.-P. Sun, *J. Am. Chem. Soc.* **2007**, *129*, 11318.
[10] D. R. Larson, W. R. Zipfel, R. M. Williams, S. W. Clark, M. P. Bruchez, F. W. Wise, W. W. Webb, *Science* **2003**, *300*, 1434.
[11] R. Liu, D. Wu, S. Liu, K. Koynov, W. Knoll, Q. Li, *Angew. Chem., Int. Ed.* **2009**, *48*, 4598.
[12] V. N. Mehta, S. Jha, S. K. Kailasa, *Mater. Sci. Eng., C* **2014**, *38*, 20.
[13] G. A. Posthuma-Trumpie, J. H. Wichers, M. Koets, L. B. J. M. Berendsen, A. van Amerongen, *Anal. Bioanal. Chem.* **2012**, *402*, 593.
[14] J. Gordon, G. Michel, *Clin. Chem.* **2008**, *54*, 1250.
[15] S. Y. Lim, W. Shen, Z. Gao, *Chem. Soc. Rev.* **2015**, *44*, 362.
[16] Y. Wang, A. Hu, *J. Mater. Chem. C* **2014**, *2*, 6921.
[17] G. Marzari, G. M. Morales, M. S. Moreno, D. I. Garcia-Gutierrez, F. Fungo, *Nanoscale* **2013**, *5*, 7977.
[18] Y.-P. Sun, B. Zhou, Y. Lin, W. Wang, K. A. S. Fernando, P. Pathak, M. J. Meziani, B. A. Harruff, X. Wang, H. Wang, P. G. Luo, H. Yang, M. E. Kose, B. Chen, L. M. Veca, S.-Y. Xie, *J. Am. Chem. Soc.* **2006**, *128*, 7756.
[19] L. Zheng, Y. Chi, Y. Dong, J. Lin, B. Wang, *J. Am. Chem. Soc.* **2009**, *131*, 4564.
[20] X. Li, H. Wang, Y. Shimizu, A. Pyatenko, K. Kawaguchi, N. Koshizaki, *Chem. Commun.* **2011**, *47*, 932.
[21] H. Liu, T. Ye, C. Mao, *Angew. Chem.* **2007**, *119*, 6593.
[22] S.-L. Hu, K.-Y. Niu, J. Sun, J. Yang, N.-Q. Zhao, X.-W. Du, *J. Mater. Chem.* **2009**, *19*, 484.
[23] S.-T. Yang, L. Cao, P. G. Luo, F. Lu, X. Wang, H. Wang, M. J. Meziani, Y. Liu, G. Qi, Y.-P. Sun, *J. Am. Chem. Soc.* **2009**, *131*, 11308.
[24] S. Hu, J. Liu, J. Yang, Y. Wang, S. Cao, *J. Nanopart. Res.* **2011**, *13*, 7247.
[25] Y. Zhang, X. Cui, F. Shi, Y. Deng, *Chem. Rev.* **2012**, *112*, 2467.
[26] J. Zeng, Q. Zhang, J. Chen, Y. Xia, *Nano Lett.* **2010**, *10*, 30.
[27] X. Zhou, N. M. Andoy, G. Liu, E. Choudhary, K.-S. Han, H. Shen, P. Chen, *Nat. Nanotechnol.* **2012**, *7*, 237.
[28] M. Comotti, C. Della Pina, R. Matarrese, M. Rossi, *Angew. Chem., Int. Ed.* **2004**, *43*, 5812.
[29] S. Kim, S. W. Bae, J. S. Lee, J. Park, *Tetrahedron* **2009**, *65*, 1461.
[30] D. A. Knight, R. Nita, M. Moore, D. Zabetakis, M. Khandelwal, B. D. Martin, J. Fontana, E. Goldberg, A. R. Funk, E. L. Chang, S. A. Trammell, *J. Nanopart. Res.* **2014**, *16*, 2400.
[31] H. Zhu, X. Chen, Z. Zheng, X. Ke, E. Jaatinen, J. Zhao, C. Guo, T. Xie, D. Wang, *Chem. Commun.* **2009**, 7524.
[32] T. Tachikawa, T. Yonezawa, T. Majima, *ACS Nano* **2013**, *7*, 263.
[33] M. F. Limonov, M. V. Rybin, A. N. Poddubny, Y. S. Kivshar, *Nat. Photonics* **2017**, *11*, 543.
[34] A. E. Miroshnichenko, Y. S. Kivshar, *Nano Lett.* **2012**, *12*, 6459.
[35] B. Luk'yanchuk, N. I. Zheludev, S. A. Maier, N. J. Halas, P. Nordlander, H. Giessen, C. T. Chong, *Nat. Mater.* **2010**, *9*, 707.
[36] Y. Cui, J. Zhou, V. A. Tamma, W. Park, *ACS Nano* **2012**, *6*, 2385.
[37] L. Khosravi Khorashad, L. V. Besteiro, Z. Wang, J. Valentine, A. O. Govorov, *J. Phys. Chem. C* **2016**, *120*, 13215.
[38] X.-J. Mao, H.-Z. Zheng, Y.-J. Long, J. Du, J.-Y. Hao, L.-L. Wang, D.-B. Zhou, *Spectrochim. Acta, Part A* **2010**, *75*, 553.
[39] Q. Wang, H. Zheng, Y. Long, L. Zhang, M. Gao, W. Bai, *Carbon* **2011**, *49*, 3134.
[40] L. Zhao, F. Di, D. Wang, L.-H. Guo, Y. Yang, B. Wan, H. Zhang, *Nanoscale* **2013**, *5*, 2655.
[41] W. Chen, S. Li, C. Chen, L. Yan, *Adv. Mater.* **2011**, *23*, 5679.
[42] J. Chen, B. Yao, C. Li, G. Shi, *Carbon* **2013**, *64*, 225.
[43] M. R. K. Ali, B. Snyder, M. A. El-Sayed, *Langmuir* **2012**, *28*, 9807.
[44] G. M. Whitesides, B. Grzybowski, *Science* **2002**, *295*, 2418.
[45] C. J. Brinker, Y. Lu, A. Sellinger, H. Fan, *Adv. Mater.* **1999**, *11*, 579.
[46] K. J. Stebe, E. Lewandowski, M. Ghosh, *Science* **2009**, *325*, 159.

